

GW190521: First Measurement of Stimulated Hawking Radiation from Black Holes

Jahed Abedi,^{1,2,3,*} Lu s Felipe Longo Micchi,^{4,†} and Niayesh Afshordi^{5,6,7,‡}

¹*Department of Mathematics and Physics, University of Stavanger, NO-4036 Stavanger, Norway*

²*Max-Planck-Institut f r Gravitationsphysik, D-30167 Hannover, Germany*

³*Leibniz Universit t Hannover, D-30167 Hannover, Germany*

⁴*Center for Natural and Human Sciences, UFABC, Santo Andr e, SP 09210-170, Brazil*

⁵*Department of Physics and Astronomy, University of Waterloo,*

200 University Ave W, N2L 3G1, Waterloo, Canada

⁶*Waterloo Centre for Astrophysics, University of Waterloo, Waterloo, ON, N2L 3G1, Canada*

⁷*Perimeter Institute For Theoretical Physics, 31 Caroline St N, Waterloo, Canada*

Being the most massive binary black hole merger event observed to date, GW190521 is in a class of its own. The exceptionally loud ringdown of this merger makes it an ideal candidate to search for gravitational wave echoes, a proposed smoking gun for the quantum structure of black hole horizons. We perform an unprecedented multi-pronged search for echoes via two well-established and independent pipelines: a template-based search for stimulated emission of Hawking radiation, or Boltzmann echoes, and the model-agnostic coherent WaveBurst (cWB) search. Stimulated Hawking radiation from the merger is expected to lead to post-merger echoes at horizon mode frequency of ~ 50 Hz (for quadrupolar gravitational radiation), repeating at intervals of ~ 1 second, due to partial reflection off Planckian quantum structure of the horizon. A careful analysis using dynamic nested sampling yields a Bayesian evidence of 7 ± 2 (90% confidence level) for this signal following GW190521, carrying an excess of $10^{+9}_{-7}\%$ in gravitational wave energy, relative to the main event. Similarly, the reconstructed waveform of the first echo in cWB carries an energy excess of $13^{+16}_{-7}\%$. Accounting for the “look-elsewhere” effects, we estimate a p-value for false detection probability of 5.1×10^{-3} (or 2.6σ) using cWB pipeline, although the verdict on the co-localization of the post-merger echo and the main event in the sky is inconclusive. While the current evidence for stimulated Hawking radiation does not reach the gold standard of 5σ , our findings are in line with expectations for stimulated Hawking radiation at current detector sensitivities. The next generation of gravitational wave observatories can thus draw a definitive conclusion on the quantum nature of black hole horizons.

Introduction.—The rise of gravitational wave (GW) astronomy has opened an unprecedented window into the mysterious nature of quantum black holes (BHs) that has fascinated theoretical physicists for nearly half a century [1, 2]. A smoking gun for the quantum structure of BH horizons, motivated by the information paradox [3, 4], is the potential appearance of GW echoes, repeating at 0.1 – 1 second intervals, that may follow detection of compact binary merger events that involve stellar BHs [5, 6]. One may consider echoes as stimulated emission of Hawking radiation, caused by the GWs that excite the quantum BH microstructure [7, 8]. While stimulated Hawking radiation has been seen in analogue BH/white hole systems, based on water waves, nonlinear optics, or Bose-Einstein condensates, for nearly a decade [9–14], they have remained elusive in real gravitational BHs.

An advantage of testing General Relativity (GR) using echoes is that while modeling the strong-field regime of mergers in modified theories of gravity is extremely challenging in Numerical Relativity, it is possible to effectively model echoes within linear perturbation theory (e.g., [15]). This provides a unique phenomenological window to search for deviations from GR, in spite of the

uncertainty in the echo templates. As GW190521 holds the record for the most massive binary BH (BBH) merger and the loudest ringdown ever detected in GWs [16–18] it can be mostly modelled perturbatively. These features make GW190521 the ideal candidate to-date to look for potential evidence for GW echoes [19], which may subsequently test many proposals for quantum nature of BHs (e.g., [5, 7, 20–22]).

Even though no evidence for deviation from GR has yet been found in LIGO/Virgo main events [23–25], tentative evidence for post-merger echoes has been reported by [26–30] (with JA and NA as co-authors on some), but they remain controversial [2, 29, 31–35]. Motivated by this, many groups have directed their efforts to search for echoes using a diverse set of tools and methodologies. So far, these searches have employed mainly two types of strategies: Template-based methods [26, 31, 36–41] and model-agnostic (or coherent) methods [27–30]. Using these approaches, different groups have drawn a range of conclusions about the existence of echoes, from positive [26–28, 30, 37] (with p-values within 0.002%–5%), to mixed [29, 31, 36], and negative evidence [37–42]. Moreover, the echoes first identified around 1 second after the binary neutron star merger GW170817 [28], coincided with the time expected for formation of a BH, subsequently inferred from electromagnetic follow-up [43].

These apparent discrepancies between different search strategies are not surprising, as different methods may

* jahed.abedi@uis.no

† luis.longo@ufabc.edu.br

‡ nafshordi@pitp.ca

be more or less effective in identifying echoes, depending on the underlying theory. For example, the search for GW190521 echoes by the LIGO/Virgo collaboration [39] (based on methodology developed in [38]) extends to a region of parameter space with nonphysical GW energy (thus diluting the evidence), while missing the physical expectation for echo time at 1 second for this event (see below), by capping $\Delta t_{\text{echo}} < 0.5$ sec. In contrast, Δt_{echo} for the boxing day event GW151226 was 0.1 second [26, 29]. This highlights the importance of using physical models as a powerful tool to guide searches for exotic physics.

In this *letter*, we adopt a more comprehensive approach to look for GW echoes by making use of different GW data analysis tools, and physical echo waveform templates. The key underlying assumption is to replace the classical event horizon by a membrane with quantum dynamics. This leads to the formation of an “echo chamber”, where GWs can be trapped between the quantum membrane and the classical angular momentum barrier, but periodically leaking out to infinity [5, 6, 19, 26, 44]. If the quantum membrane sits at a proper distance of l_{QG} away from the would-be horizon, individual echoes will be temporally separated by:

$$\Delta t_{\text{echo}} \simeq \frac{4GM_{\text{BH}}}{c^3} \left(1 + \frac{1}{\sqrt{1-a^2}}\right) \times \ln\left(\frac{M_{\text{BH}}}{\Lambda^{-1}M_{\text{planck}}}\right) \quad (1)$$

where M_{BH} and a are the final redshifted mass and dimensionless spin of the BH remnant, while $\Lambda = l_{\text{P}}/l_{\text{QG}}$ represents the ratio of the energy scale of the quantum membrane physics to the Planck scale. While we expect $\Lambda \sim 1$ for Planckian echoes, we do vary this parameter within $-13 \leq \log_{10} \Lambda \leq 13^1$. For the GW190521 BH mass and spin, we find $\Delta t_{\text{echo}}|_{\Lambda=1} = 1.1 \pm 0.3$ sec (at 90% confidence), which may explain why no echoes were found by the LIGO/Virgo collaboration [39] assuming a $0.05 \text{ sec} \leq \Delta t_{\text{echo}} \leq 0.5 \text{ sec}$ prior. We shall instead use the physical prediction (1), which fixes Δt_{echo} in terms of the final BH parameters and the scale of new physics.

The next important ingredient is a physical model for the emission of echoes. If we consider Hawking radiation as the quantum *spontaneous* emission of light particles with $\hbar\omega \sim kT_H$ from a quantum BH (e.g., fuzzballs [47, 48]) in vacuum, it is natural to expect *stimulated emission* to happen, if we immerse the BH in a classical radiation field with similar frequencies. Indeed, [7, 8] proposed this as a natural mechanism to produce echoes of GWs, showing that quantum horizons should have a flux reflectivity, given by a Boltzmann factor, $\exp(-\hbar|\omega|/kT_H)$ (in their comoving frame), through quantum stimulated emission. For observers at infinity, we have to shift the frequency $\omega \rightarrow \omega - m\Omega_H$, where Ω_H

and m are the horizon angular frequency and azimuthal harmonic number, respectively.

While one cannot produce a precise template without a quantum simulation of BBH merger, a plausible ansatz for the expected radiation is given as a sum over Boltzmann echoes:

$$h_{\text{GR+echoes}}(\omega) = h_{\text{GR}}(\omega) \left[1 + Ae^{i\phi} \sum_{n=1}^{\infty} \mathcal{R}^n\right], \quad (2)$$

$$\mathcal{R} \equiv \mp \exp\left[-\frac{\hbar|\omega - 2\Omega_H|}{2kT_H} + i\omega\Delta t_{\text{echo}}\right], \quad (3)$$

where $Ae^{i\phi}$ quantifies their overall amplitude, while the modulus and phase of \mathcal{R} quantify their relative damping and temporal separation, respectively. Generally, we expect $0 \lesssim A \lesssim 2$ and $0 < \phi \leq 2\pi$ due to GR nonlinearities. Furthermore, as is often done, we have assumed that the energy in BBH ringdown and echoes are dominated by quadrupolar radiation at $\ell = m = 2$.

In this work, for the first time we search for a physical model of stimulated Hawking radiation, and use two well-established analysis packages in order to cross-validate our findings: the template-based PyCBC [49, 50] and model-agnostic coherent WaveBurst (cWB) [51]. We thus can evaluate the statistical significance and energy of the post-merger signal in independent and complementary ways, also quantifying the evidence for the event and its post-merger trigger to be co-located. Data for these independent searches available at [52].

Search for Stimulated Hawking Radiation.—We first used the PyCBC inference [49] pipeline with the dynamic nested sampling MCMC algorithm *dynesty* [53]. The samplers serve as a way to map the hypothesis’ posterior probability distribution in the parameter space for a given dataset. Provided the likelihood function and the prior, it is possible to measure the evidence in favor of (or against) the existence of a signal in the data. During this process, it is assumed a Gaussian background, and the three detector network H1-L1-V1 is used.

In order to quantify evidence for echoes in data, we first obtained the Bayes factor for a given template (based on GR, with and without echoes) against Gaussian noise. The Bayesian evidence for stimulated Hawking radiation, or Boltzmann echoes, is then given by the ratio of Bayes factors for $h_{\text{GR+echoes}}(\omega)$ (Eq.2) over the Bayes factor of the pure GR template, $h_{\text{GR}}(\omega)$. For the latter, we adopt the NRSur7dq4 surrogate waveform.

Our analysis suggests a statistical preference for stimulated Hawking radiation: Starting with different MCMC seeds, we obtain a Bayes factor of $\mathcal{B} = 7 \pm 2$ (Fig.3), at 90% of confidence. Results obtained by using different GR surrogate waveforms and/or echo models are reported in [45]. We also noticed that, depending on the choice of GR waveform and/or priors, we may have preference for either Planckian (Fig.1a) or super-Planckian echoes: $\log_{10} \Lambda = 6.5 \pm 3.5$ or additional time delay of $(4.8 \pm 2.6) \hbar k^{-1} T_H^{-1}$ (Fig.3; see also [45]). This is due to

¹ This may alternatively be attributed to $\pm 10 \hbar k^{-1} T_H^{-1}$ uncertainty in stimulated emission time, where T_H is the Hawking temperature.

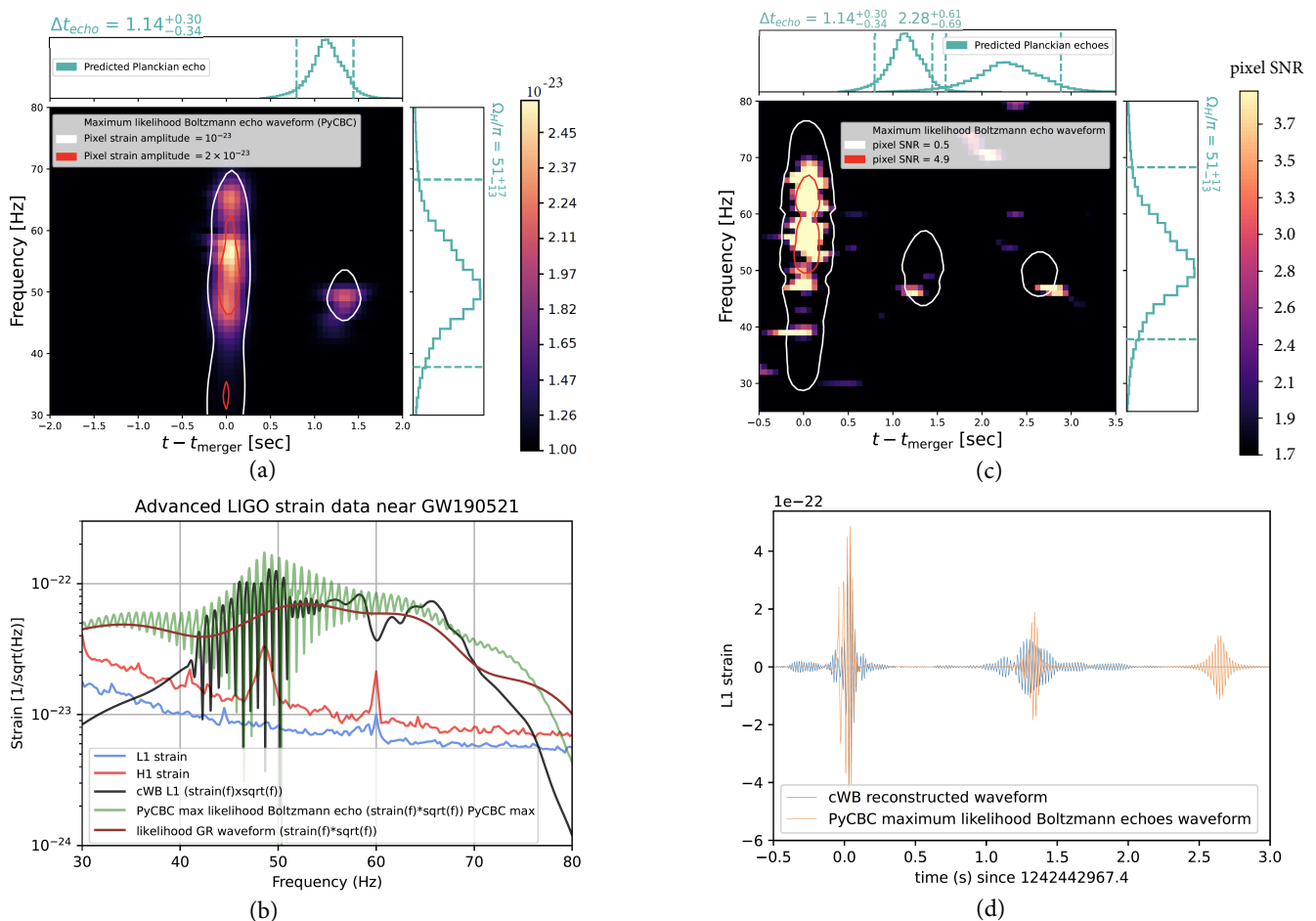


FIG. 1: (a,c): White and red contours represent the maximum likelihood Boltzmann echoes (NRSur7dq4). The light-sea-green histograms show the *predicted* 1D distributions for the 1st and 2nd Planckian echoes, based on the GR best-fit to GW190521. (a): cWB’s reconstructed waveform spectrogram compared to the maximum likelihood Boltzmann echo waveform (contours) using PyCBC assuming Planckian echoes for stimulated Hawking radiation. (b): Amplitude Spectral Density (ASD) from the reconstructed waveform as obtained by cWB (PyCBC). Here, the repeating pattern for echoes in real time leads to the oscillatory pattern in the frequency domain. (c): Whitened H1 \times L1 cross-spectrogram and predicted Planckian echoes for stimulated Hawking radiation (see [45] for details of this method). (d): Comparison between cWB’s and PyCBC’s waveforms.

degeneracy between Λ and the final BH mass, which can be seen in Fig.3.

Coherent WaveBurst (cWB) search.—As an independent method, we then used the model-agnostic cWB package to test the robustness of the evidence for echoes.

The cWB package is a pipeline specialized in reconstructing GW signals by making minimal assumptions regarding the waveform morphology. To perform such reconstruction, we start by searching for burst of energy excess that are coherent (coherent energy E_C), in the time-frequency domain, in multiple detectors. During its workflow, the software defines a coherence statistics that is related to the signal-to-noise ratio (SNR) in the detector. Once the waveform is estimated, it is subtracted from the data and the null energy E_N is estimated. As a measure of the coherence of the signal the network

correlation coefficient as $cc = E_C/(E_C + E_N)$, which satisfies $0 \leq cc \leq 1$. The cc parameter is one of the multiple search thresholds that triggers have to satisfy, usually $cc > 0.7$ is required to claim a potential detection. As final products, cWB is capable of producing a reconstructed waveform and sky-location analysis.

We first reproduce GW190521 main event’s detection (see Fig.2a) in agreement with Fig.2 of [46]. We reconstruct the spectrogram of the event+post-merger echoes using all the recommended search parameters [54], but allowing for separations of $\gtrsim 1$ second (Fig.2b). In order to quantify their significance and sky-location, we can further subtract the best-fit GR template from the strain data and look for the echo-only cWB signal with lower thresholds (Fig.2c). The comparison between the reconstructed model-agnostic waveform (cWB) and the best-

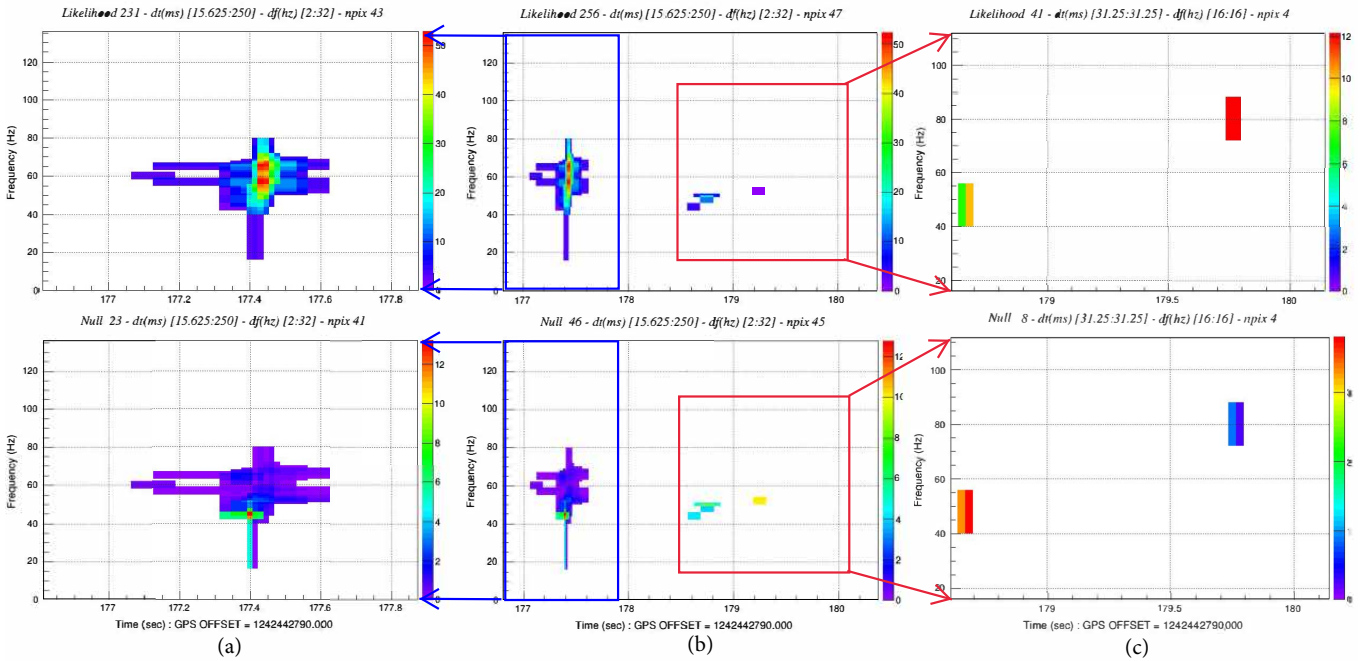


FIG. 2: cWB color-coded time-frequency maps for GW190521. Left (compare to [46]) and middle panels were obtained by using the recommended LVK thresholds on the original data. Right panels were obtained by using the weaker thresholds on the GR subtracted data. The middle panels differ from the left ones mainly by the time length of the search. Top panels show the likelihood, which is related to the coherent energy between detectors, E_C , while the bottom lines show the null energy E_N (see text for details).

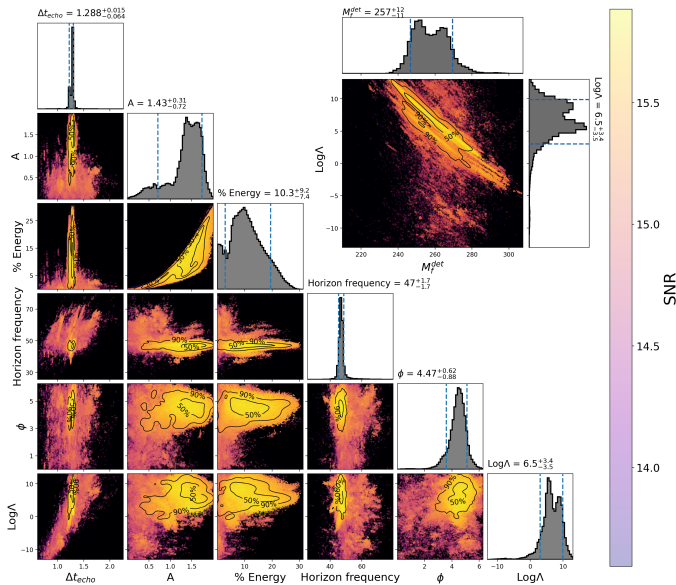


FIG. 3: Parameter estimation of Boltzmann echo waveform using NRSur7dq4. We find Bayes factor of $\mathcal{B} = 7 \pm 2$ in preference for echoes.

fit stimulated Hawking radiation waveform (PyCBC) can be seen in Figs. 1a and 1b (high thresholds) and 1c (low thresholds). We notice that (apart from a rogue pixel at ≈ 80 Hz for the lower threshold search), both methods

	cWB $\mathcal{B}_{ab}^{\text{co-loc}}$			cWB			PyCBC
	Joint	Main event	Echo	ρ	cc	SNR	SNR
Joint	51.88	46.20	0.32	10.6	0.90	16.0	16
Main event	46.20	42.51	0.40	10.8	0.95	15.2	15
Echo	0.32	0.40	37.98	4.1	0.88	4.1	6 ^a

^a Based on search for echoes without including main event

TABLE I: Collection of several statistical findings. Here cc quantifies the degrees of signal coincidence amongst detectors ($0 \leq cc \leq 1$), while ρ is the so-called the effective correlated SNR (see [29]). While the evidence of 0.4 for co-localization is inconclusive, we notice an improvement of $\approx 22\%$ in the Bayes factor for self-localization of the event when including the post-merger signal.

achieve qualitatively consistent post-merger waveforms. Given this analysis, we obtained not only the event's spectrogram but also its sky localization and its statistical significance, both the main event and post-merger signal (see Table I).

The energy estimation using two independent methods are also in agreement $10_{-7}^{+9}\%$ and $13_{-7}^{+16}\%$ for PyCBC and cWB respectively (see [45] for further details).

While the signal-to-noise ratio for echoes is not very large (4.1/6 for echoes in cWB/PyCBC, compared to 15 for the main event; see Table I), it is in line with what is expected for stimulated Hawking radiation from

an event with $\text{SNR}_{\text{ringdown}} \sim 16$, which is $\text{SNR}_{\text{echo}}=2.5$ (Fig.9 in [19] for mass ratio $q \sim 0.8$ [16])

In order to estimate the background, we obtain the p-values in two independent ways. Via an injection study we achieved a p-value of 5.1×10^{-3} (2.6σ), and when searching for triggers in subtracted data the value found was 1.6×10^{-4} (3.6σ ; see [45] for details).

Sky co-localization.—Using the cWB sky localization posterior map, we could compute the Bayes factor for the co-localization hypothesis for signals a and b as:

$$\mathcal{B}_{ab}^{\text{co-loc}} = N \sum_{i=1}^N P_a(\phi_i, \theta_i) P_b(\phi_i, \theta_i) \quad (4)$$

where $P_a(\phi_i, \theta_i)$ is the posterior probability of event a being located within the i -th of the N pixels of the skymap [45]. We validated this method by injecting waveforms containing echoes. For loud echo injections, we find positive evidence for co-localization. However, as to the real data, we find an “inconclusive” Bayes factor of 0.4 for the co-localization of cWB main event and echoes (Table I). We further see that random noise generates triggers that have evidence in favor of the co-localization one quarter of the time, suggesting the limited power of localization information in differentiating events in the sky at this SNR-level [45]. As we noted above in Fig.2c, we notice that lowering the cWB thresholds picks up a possible noise feature at 80 Hz (absent for the high threshold search), which could be interfering on our sky localization analysis. To avoid this, we can compare the Bayes factors for the self-localization (diagonal entries on Table I cWB $\mathcal{B}_{ab}^{\text{co-loc}}$) for the joint analysis (event+echo) and the main event. Addition of the echo improves self-localization Bayes factor by $\approx 22\%$. This suggests that excluding the 80 Hz noise feature (as in Fig.2b) leads to marginal evidence for co-localization hypothesis.

Conclusion.—Using two independent and complementary approaches to GW search (PyCBC and cWB) we found positive evidence for the presence of stimulated Hawking radiation, or post-merger Boltzmann echoes in the aftermath of GW190521 BBH merger. Bayesian evidence for echoes is 7 ± 2 (via PyCBC), while the frequentist evidence can be quantified by p-value= 5.1×10^{-3} or 1.6×10^{-4} (via different cWB implementations). However, at the current level of signal-to-noise ratio, the evidence for the co-localization of the echoes and the main event in the sky remains inconclusive.

We also argued that previous searches (e.g., [39] by the LIGO/Virgo collaboration) have missed this signal due to a nonphysical prior range, notably missing the expected $\Delta t_{\text{echo}} = 1.14_{-0.34}^{+0.30}$ sec for GW190521, with their choice of $0.05 \text{ sec} < \Delta t_{\text{echo}} < 0.5 \text{ sec}$ prior.

We conclude by noting that no indisputable evidence ($\geq 5\sigma$) for stimulated Hawking radiation from BH mergers, or Boltzmann echoes, were to be expected at current levels of GW detector sensitivity [19]. From a conservative standpoint, current analysis provides the best constraint on the energy and morphology of this signal to

date. The fact that independent methods find similar signals suggests that echoes should be a prime target for the next generation of GW detectors.

Acknowledgements.—We thank Cecilia Chirenti, Randy Conklin, Cole Miller, Germano Nardini, Alex B. Nielsen, and Francesco Salemi for useful discussions. JA thanks the Max Planck Gesellschaft and the Atlas cluster computing team at AEI Hannover for support and computational help. JA was supported by ROM-FORSK grant Project. No. 302640. LFLM thanks the financial support of the São Paulo Research Foundation (FAPESP) grant 2017/24919-4 and of Coordenação de Aperfeiçoamento de Pessoal de Nível Superior- Brasil (Capes) - Finance code 001 through the Capes-PrInt program, and thanks Perimeter Institute for the access to its cluster. NA is supported by the University of Waterloo, Natural Sciences and Engineering Research Council of Canada (NSERC) and the Perimeter Institute for Theoretical Physics. Research at Perimeter Institute is supported in part by the Government of Canada through the Department of Innovation, Science and Economic Development Canada and by the Province of Ontario through the Ministry of Colleges and Universities. This research has made use of data, software and/or web tools obtained from the GW Open Science Center (<https://www.gw-openscience.org>), a service of LIGO Laboratory, the LIGO Scientific Collaboration and the Virgo Collaboration. LIGO is funded by the U.S. National Science Foundation. Virgo is funded by the French Centre National de Recherche Scientifique (CNRS), the Italian Istituto Nazionale della Fisica Nucleare (INFN) and the Dutch Nikhef, with contributions by Polish and Hungarian institutes.

-
- [1] V. Cardoso and P. Pani, *Living Rev. Rel.* **22**, 4 (2019), [arXiv:1904.05363 \[gr-qc\]](https://arxiv.org/abs/1904.05363).
 - [2] J. Abedi, N. Afshordi, N. Oshita, and Q. Wang, *Universe* **6**, 43 (2020), [arXiv:2001.09553 \[gr-qc\]](https://arxiv.org/abs/2001.09553).
 - [3] A. Almheiri, D. Marolf, J. Polchinski, and J. Sully, *JHEP* **02**, 062 (2013), [arXiv:1207.3123 \[hep-th\]](https://arxiv.org/abs/1207.3123).
 - [4] J. Polchinski, in *The Black Hole Information Problem* (2017) pp. 353–397, [arXiv:1609.04036 \[hep-th\]](https://arxiv.org/abs/1609.04036).
 - [5] V. Cardoso, E. Franzin, and P. Pani, *Phys. Rev. Lett.* **116**, 171101 (2016), [Erratum: *Phys. Rev. Lett.* 117, no.8, 089902(2016)], [arXiv:1602.07309 \[gr-qc\]](https://arxiv.org/abs/1602.07309).
 - [6] V. Cardoso, S. Hopper, C. F. B. Macedo, C. Palenzuela, and P. Pani, *Phys. Rev.* **D94**, 084031 (2016), [arXiv:1608.08637 \[gr-qc\]](https://arxiv.org/abs/1608.08637).
 - [7] N. Oshita, Q. Wang, and N. Afshordi, *JCAP* **04**, 016 (2020), [arXiv:1905.00464 \[hep-th\]](https://arxiv.org/abs/1905.00464).
 - [8] Q. Wang, N. Oshita, and N. Afshordi, (2019), [arXiv:1905.00446 \[gr-qc\]](https://arxiv.org/abs/1905.00446).
 - [9] S. Weinfurtner, E. W. Tedford, M. C. J. Penrice, W. G. Unruh, and G. A. Lawrence, *Phys. Rev. Lett.* **106**, 021302 (2011), [arXiv:1008.1911 \[gr-qc\]](https://arxiv.org/abs/1008.1911).
 - [10] J. Steinhauer, *Nature Phys.* **10**, 864 (2014), [arXiv:1409.6550 \[cond-mat.quant-gas\]](https://arxiv.org/abs/1409.6550).

- [11] Y.-H. Wang, T. Jacobson, M. Edwards, and C. W. Clark, *Phys. Rev. A* **96**, 023616 (2017), [arXiv:1605.01027 \[cond-mat.quant-gas\]](#).
- [12] J. Drori, Y. Rosenberg, D. Bermudez, Y. Silberberg, and U. Leonhardt, *Phys. Rev. Lett.* **122**, 010404 (2019), [arXiv:1808.09244 \[gr-qc\]](#).
- [13] A. Bera and S. Ghosh, *Phys. Rev. D* **101**, 105012 (2020), [arXiv:2001.08467 \[hep-th\]](#).
- [14] J. Steinhauer, (2021), [arXiv:2110.06796 \[gr-qc\]](#).
- [15] C. P. Burgess, R. Plestid, and M. Rummel, *JHEP* **09**, 113 (2018), [arXiv:1808.00847 \[gr-qc\]](#).
- [16] R. Abbott et al. (LIGO Scientific, Virgo), *Phys. Rev. Lett.* **125**, 101102 (2020), [arXiv:2009.01075 \[gr-qc\]](#).
- [17] R. Abbott et al. (LIGO Scientific, Virgo), *Astrophys. J. Lett.* **900**, L13 (2020), [arXiv:2009.01190 \[astro-ph.HE\]](#).
- [18] C. D. Capano, M. Cabero, J. Westerweck, J. Abedi, S. Kastha, A. H. Nitz, A. B. Nielsen, and B. Krishnan, (2021), [arXiv:2105.05238 \[gr-qc\]](#).
- [19] L. F. Longo Micchi, N. Afshordi, and C. Chirenti, *Phys. Rev. D* **103**, 044028 (2021), [arXiv:2010.14578 \[gr-qc\]](#).
- [20] V. Cardoso, V. F. Foit, and M. Kleban, *JCAP* **08**, 006 (2019), [arXiv:1902.10164 \[hep-th\]](#).
- [21] P. Hayden and G. Penington, (2020), [arXiv:2012.07861 \[hep-th\]](#).
- [22] T. Ikeda, M. Bianchi, D. Consoli, A. Grillo, J. F. Morales, P. Pani, and G. Raposo, *Phys. Rev. D* **104**, 066021 (2021), [arXiv:2103.10960 \[gr-qc\]](#).
- [23] B. P. Abbott et al. (Virgo, LIGO Scientific), *Phys. Rev. Lett.* **116**, 221101 (2016), [arXiv:1602.03841 \[gr-qc\]](#).
- [24] B. P. Abbott et al. (LIGO Scientific, VIRGO), *Phys. Rev. Lett.* **118**, 221101 (2017), [Erratum: *Phys. Rev. Lett.* 121,no.12,129901(2018)], [arXiv:1706.01812 \[gr-qc\]](#).
- [25] B. P. Abbott et al. (LIGO Scientific, Virgo), *Phys. Rev. Lett.* **123**, 011102 (2019), [arXiv:1811.00364 \[gr-qc\]](#).
- [26] J. Abedi, H. Dykaar, and N. Afshordi, *Phys. Rev. D* **96**, 082004 (2017), [arXiv:1612.00266 \[gr-qc\]](#).
- [27] R. S. Conklin, B. Holdom, and J. Ren, *Phys. Rev. D* **98**, 044021 (2018), [arXiv:1712.06517 \[gr-qc\]](#).
- [28] J. Abedi and N. Afshordi, *JCAP* **1911**, 010 (2019), [arXiv:1803.10454 \[gr-qc\]](#).
- [29] F. Salemi, E. Milotti, G. A. Prodi, G. Vedovato, C. Lazzaro, S. Tiwari, S. Vinciguerra, M. Drago, and S. Klimentko, *Phys. Rev. D* **100**, 042003 (2019), [arXiv:1905.09260 \[gr-qc\]](#).
- [30] B. Holdom, *Phys. Rev. D* **101**, 064063 (2020), [arXiv:1909.11801 \[gr-qc\]](#).
- [31] J. Westerweck, A. Nielsen, O. Fischer-Birnholtz, M. Cabero, C. Capano, T. Dent, B. Krishnan, G. Meadors, and A. H. Nitz, *Phys. Rev. D* **97**, 124037 (2018), [arXiv:1712.09966 \[gr-qc\]](#).
- [32] G. Ashton, O. Birnholtz, M. Cabero, C. Capano, T. Dent, B. Krishnan, G. D. Meadors, A. B. Nielsen, A. Nitz, and J. Westerweck, (2016), [arXiv:1612.05625 \[gr-qc\]](#).
- [33] J. Abedi, H. Dykaar, and N. Afshordi, (2017), [arXiv:1701.03485 \[gr-qc\]](#).
- [34] J. Abedi, H. Dykaar, and N. Afshordi, (2018), [arXiv:1803.08565 \[gr-qc\]](#).
- [35] J. Abedi and N. Afshordi, (2020), [arXiv:2001.00821 \[gr-qc\]](#).
- [36] A. B. Nielsen, C. D. Capano, O. Birnholtz, and J. Westerweck, *Phys. Rev. D* **99**, 104012 (2019), [arXiv:1811.04904 \[gr-qc\]](#).
- [37] N. Uchikata, H. Nakano, T. Narikawa, N. Sago, H. Tagoshi, and T. Tanaka, *Phys. Rev. D* **100**, 062006 (2019), [arXiv:1906.00838 \[gr-qc\]](#).
- [38] R. K. L. Lo, T. G. F. Li, and A. J. Weinstein, *Phys. Rev. D* **99**, 084052 (2019), [arXiv:1811.07431 \[gr-qc\]](#).
- [39] R. Abbott et al. (LIGO Scientific, Virgo), (2020), [arXiv:2010.14529 \[gr-qc\]](#).
- [40] Y.-T. Wang and Y.-S. Piao, (2020), [arXiv:2010.07663 \[gr-qc\]](#).
- [41] J. Westerweck, Y. Sherf, C. D. Capano, and R. Brustein, (2021), [arXiv:2108.08823 \[gr-qc\]](#).
- [42] K. W. Tsang, A. Ghosh, A. Samajdar, K. Chatziioannou, S. Mastrogiovanni, M. Agathos, and C. Van Den Broeck, (2019), [arXiv:1906.11168 \[gr-qc\]](#).
- [43] R. Gill, A. Nathanail, and L. Rezzolla, *Astrophys. J.* **876**, 139 (2019), [arXiv:1901.04138 \[astro-ph.HE\]](#).
- [44] Q. Wang and N. Afshordi, *Phys. Rev. D* **97**, 124044 (2018), [arXiv:1803.02845 \[gr-qc\]](#).
- [45] “Supplemental material,” attached below.
- [46] M. Szczepańczyk, S. Klimentko, B. O’Brien, I. Bartos, V. Gayathri, G. Mitselmakher, G. Prodi, G. Vedovato, C. Lazzaro, E. Milotti, F. Salemi, M. Drago, and S. Tiwari, *Phys. Rev. D* **103**, 082002 (2021).
- [47] O. Lunin and S. D. Mathur, *Nucl. Phys. B* **623**, 342 (2002), [arXiv:hep-th/0109154 \[hep-th\]](#).
- [48] O. Lunin and S. D. Mathur, *Phys. Rev. Lett.* **88**, 211303 (2002), [arXiv:hep-th/0202072 \[hep-th\]](#).
- [49] C. M. Biwer, C. D. Capano, S. De, M. Cabero, D. A. Brown, A. H. Nitz, and V. Raymond, *Publ. Astron. Soc. Pac.* **131**, 024503 (2019), [arXiv:1807.10312 \[astro-ph.IM\]](#).
- [50] A. Nitz, I. Harry, D. Brown, C. M. Biwer, J. Willis, T. D. Canton, C. Capano, T. Dent, L. Pekowsky, A. R. Williamson, G. S. C. Davies, S. De, M. Cabero, B. Machenschalk, P. Kumar, D. Macleod, S. Reyes, dfinstad, F. Pannarale, T. Massinger, S. Kumar, M. Tápai, L. Singer, S. Khan, S. Fairhurst, A. Nielsen, S. Singh, K. Chandra, shasvath, and B. U. V. Gadre, “gwastro/pycbc,” (2021).
- [51] S. Klimentko, G. Vedovato, V. Necula, F. Salemi, M. Drago, E. Chassande-Mottin, V. Tiwari, C. Lazzaro, B. O’Brien, M. Szczepańczyk, S. Tiwari, and V. Gayathri, “cwb pipeline library: 6.4.0,” (2021).
- [52] “PyCBC, cWB and cross-correlation data,” <https://github.com/No-GAP/GW190521echo> ().
- [53] J. S. Speagle, *Monthly Notices of the Royal Astronomical Society* **493**, 3132–3158 (2020).
- [54] “coherent waveburst,” <https://gwburst.gitlab.io>.
- [55] J. M. Ezquiaga and M. Zumalacárregui, *Phys. Rev. D* **102**, 124048 (2020), [arXiv:2009.12187 \[gr-qc\]](#).
- [56] “Binary black hole signals in ligo open data,” https://losc.ligo.org/s/events/GW150914/LOSC_Event_tutorial_GW150914.html ().

Supplemental Material

A: Co-localization

Here, we prove Equation 4. The two hypotheses are:

1. H_0 : The two events are not co-localized
2. H_1 : The two events are co-localized

The Bayes factor is defined as:

$$\begin{aligned} \mathcal{B}^{\text{co-loc}} &\equiv \frac{\mathcal{L}(\text{data}|H_1)}{\mathcal{L}(\text{data}|H_0)} \\ &= \frac{\sum_{p_1} \mathcal{L}(\text{data}|H_1, p_1)P(H_1, p_1)}{\sum_{p_0} \mathcal{L}(\text{data}|H_0, p_0)P(H_0, p_0)}, \end{aligned} \quad (5)$$

where \mathcal{L} functions quantify the likelihood of recovering “data” within a given hypothesis, while p_0 and p_1 are the parameters of the models, with priors $P(\dots)$, within hypotheses H_0 and H_1 , respectively. In particular, p_0 would be the sky locations of the two independent events $(\phi_i, \theta_i, \phi_j, \theta_j)$, while p_1 is the sky location of a single event (ϕ_i, θ_i) . Therefore, the likelihood functions are related to the sky maps:

$$\mathcal{L}(\text{data}|H_0, p_0) = P_1(\phi_i, \theta_i)P_2(\phi_j, \theta_j), \quad (6)$$

$$\mathcal{L}(\text{data}|H_1, p_1) = P_1(\phi_i, \theta_i)P_2(\phi_i, \theta_i). \quad (7)$$

Meanwhile, assuming uniform priors across the sky in either case implies:

$$P(H_0, p_0) = N^{-2}, P(H_1, p_1) = N^{-1}, \quad (8)$$

for N pixels in the sky. Therefore,

$$\begin{aligned} \mathcal{B}^{\text{co-loc}} &= \frac{N \sum_i P_1(\phi_i, \theta_i)P_2(\phi_i, \theta_i)}{(\sum_i P_1(\phi_i, \theta_i)) \times (\sum_j P_2(\phi_j, \theta_j))} \\ &= N \sum_{i=1}^N P_1(\phi_i, \theta_i)P_2(\phi_i, \theta_i), \end{aligned} \quad (9)$$

where in the last line we used the fact that P_1 and P_2 are normalized across the sky. \square

The sky probability maps for GW190521 main event and echo can be compared in Fig.4a. In Fig.4b, we show the survivor density function found for the Bayes factors of the 51 triggers due to noise found during our p-values estimation (see Appendix B).

B: cWB p-value estimation

In this section, we quantify the p-value of pixels in cWB using two methods with a conservative approach using injections of GR waveform, and a less conservative approach with subtracting the main event.

With the injection approach we inject the maximum likelihood GR waveform in random places within

$-32 \text{ sec} < t - t_{\text{merger}} < 32 \text{ sec}$ excluding $-5 \text{ sec} < t - t_{\text{merger}} < 5 \text{ sec}$ for a data for which the main event was already subtracted (to avoid any confusion for cWB search). In order to get better realizations of noise (off-source data) we also randomly time-shifted each detector data independently with maximum allowed shifts between -3 sec to $+3 \text{ sec}$. The search is implemented any time we inject the maximum likelihood GR waveform of the event for both user parameters of Figs. 2a (up to 0.5 second post-merger) and 2b (up to 3 seconds post-merger). The comparison of SNR^2 of the two identified cWB triggers quantifies the significance of cWB echoes. As this difference is $24.3 = 15.98^2 - 15.20^2$ for the real event (Table I), we can estimate a p-value based on the number of times that ΔSNR^2 exceeds this in random injections. Assuming that with almost equal chance backward and forward echoes may appear in random noise, we exclude the backward pulses from our look-elsewhere search, yielding a p-value $= 5.1_{-2.2}^{+2.2} \times 10^{-3}$ (see Fig.5).

For the subtraction approach, after subtracting the best-fit from the original data, we lowered cWB’s search parameters in order to accomplish a independent detection of the tentative post-merger signal, resulting in Fig.2c. The follow up question is how likely are we to detect triggers meeting the same thresholds on stretches of data where no signal is known to exist, in other words, how likely is random noise to produce similar signals. To address such question we performed the following procedure. Using ($L=$)1200 seconds of data around the main event for three detector (Livingston, Hanford and Virgo) we perform searches with the same cWB’s search parameters that lead to the tentative echo detection on synthetic data. Our synthetic data was created by temporally shifting different detectors data streams with respect to the others. A total of ($n=$)271 time shifts were performed in multiple steps of 1 second, thus effectively creating ≈ 3.8 days of data. During the search for triggers in the noisy data ($m=$)51 triggers were found. As we expect successive echoes to be apart for no more than 1 second ($\Delta t_{\text{echo}} \approx 1 \text{ sec}$) we assumed the signal’s average length to be the same. For those familiar to cWB pipeline, this means that we set the Tgap parameter to be 1 second. Given this parameters we estimated the p-value as:

$$\text{p-value} = \frac{m \times \Delta t_{\text{echo}}}{L \times n}, \quad (10)$$

where for our particular case we find p-value $= 1.6 \times 10^{-4}$, which correspond to a confidence level of 3.6σ .

The attentive reader may note an apparent inconsistency between the Bayes factor found via PyCBC and the p-value computed via cWB. The reason behind this illusory paradox is that these numbers answer two very different questions. While the Bayes factor quantifies the Bayesian statistical support for the existence of echoes *after* the GW190521 event for *the specific* Boltzmann model, the aforementioned p-value gives us a frequentist model-agnostic probability of finding a trigger with

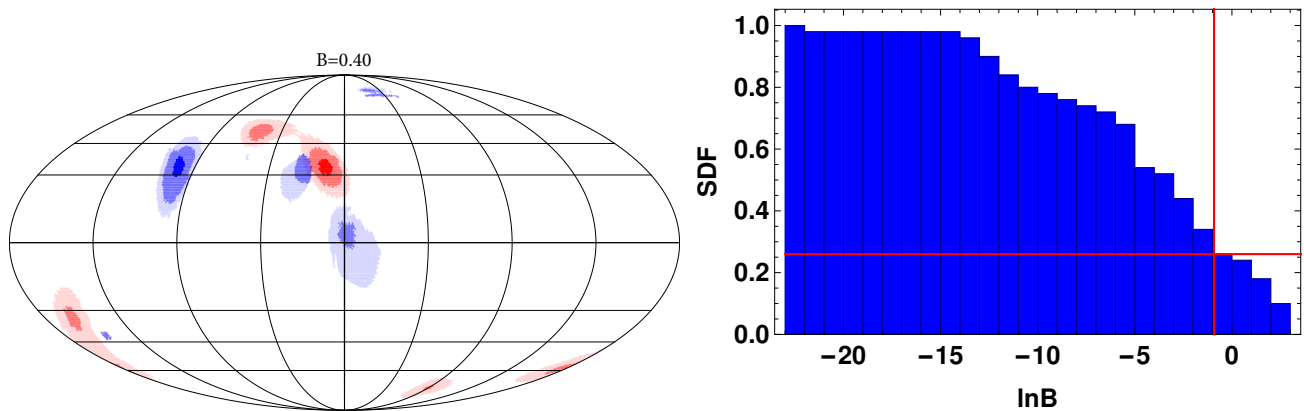


FIG. 4: Left: Sky localization comparison. Here the different opacities represent the 10-50-90% confidence regions in the sky. Red and blue areas represent the main event and echo (obtained after subtracting the main event), respectively. We notice that our main event results are in agreement with [46]. Sky localization analysis for cWB echoes, showing inconclusive evidence for/against the co-localization of the main event and the echoes, with a Bayes factor of $\mathcal{B}^{\text{co-loc}} \simeq 0.4$. Right: Cumulative distribution function for the co-localization Bayes factors for all noise triggers found during the p-value estimation (see Appendix B). Red lines mark the Bayes factor found for the post-merger signal. The PDF holds a mean of ≈ -4.87 and a standard deviation of ≈ 5.69 .

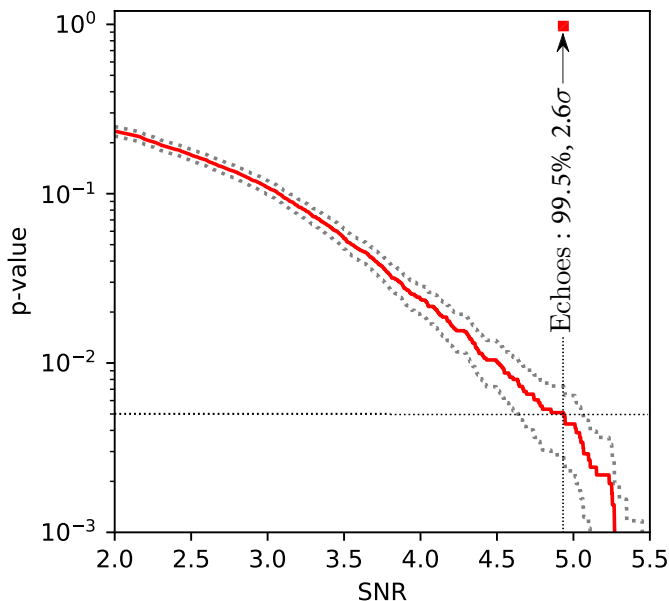


FIG. 5: cWB p-value estimation postmerger signal vs its signal-to-noise ratio and its Poisson error using injection approach.

similar cWB significance to recovered echoes, from random noise, i.e. a measure of the “look-elsewhere” effect. Therefore, there is no reason to expect them to represent same confidence levels.

C: Energy estimation of echoes in cWB

One of cWB’s capabilities is the reconstruction of the signal based on the excess of coherent energy in the network detectors. During our analysis of GW190521 we perform such reconstruction, which is shown in Fig.1d. In this process, cWB reconstructs the waveform as seen by each one of the network detectors. In order to estimate the energy of the physical strain, we perform the following calculation:

$$E \approx \int f^2 \frac{\sum_i |h_i(f)|^2 S_i^{-2}(f) df}{\sum_i S_i(f)^{-2} df} \quad (11)$$

where the sum is over the detector network, $S_i(f)$ and $h_i(f)$ is the noise ASD and the observed strain at the i -th detector respectively. The integral was performed between 0 and 100 Hz, which is a reasonable range, given the results found in Fig.8a. Equation (11) is a way of weighting (or whitening) the contribution of the individual detector regarding its strain sensitivity. In order to compute the percentage of energy in the echo part of the waveform we compute:

$$E_{\text{echo}}(\%) = \frac{E_{\text{full}} - E_{\text{main}}}{E_{\text{main}}}, \quad (12)$$

which is the value quoted in Table II as equal to 13.8%. As this value was reconstructed via cWB we will refer to it as recovered energy. The next task is to estimate the error on the “true” energy, given the value of the recovered energy.

Our starting point for estimating the error on $E_{\text{echo}}(\%)$ is injecting 600 waveforms in noisy data around

$E_{\text{MainEvent}}^{\text{Echoes}}$	L1	H1	V1	Mean
cWB ^{Rec.}	15.3%	10.8%	6.6%	13.8%
cWB ^{Inj.}	-	-	-	$13_{-7}^{+16}\%$
PyCBC	-	-	-	$10_{-7}^{+9}\%$

TABLE II: Energy ratio of the first echo with respect to the main event. cWB estimate was obtained from the reconstructed frequency-domain waveforms as in Fig.2a and 2b, and the mean of the energies is given by weighting the waveforms by the noise ASD², see Equation 11.

GW190521 event (± 32 s.), after subtracting the main event. The injected waveforms $h_i^{\text{inj.}}(t)$ are constructed by using the reconstructed strain by cWB $h_i^{\text{rec.}}(t)$ as follows:

$$h_i^{\text{inj.}}(t) = h_i^{\text{rec.}}(t)(1 + \alpha\Theta(t - t_1)\Theta(t_2 - t)) \quad (13)$$

for $t_2 > t_1$. In equation (13), the i index represents the detector, $\Theta(t)$ is the Heaviside step function and $t_2 = t_{\text{echo}} + 1.25$ and $t_1 = t_{\text{echo}} - 0.75$ are chosen such that only the echo part of the waveform is modified. The extra parameter α is sampled from -1 to 2, in a way to be more densely populated between -1 and 0.5. As the energy is quadratic on the strain, our method is equivalent to inject wave with energies of:

$$E_{\text{echo}}^{\text{inj.}}(\%) = E_{\text{echo}}^{\text{rec.}}(\%)(1 + \alpha)^2, \quad (14)$$

where $E_{\text{echo}}^{\text{rec.}}(\%) = 13.8\%$, as obtained from cWB in real data.

After performing the injections, we perform similar searches to the one leading to Fig.2b and computed the echo energy for each injection via equations (11-12). Our goal is to determine the dispersion of the measured energy, provided a prior knowledge of the existing signal on the data. After performing the search with selecting only events which reconstructed echo energy above between 5 and 63%. This selection was made in order to eliminate the case with no clear echo detection and to avoid selection bias due to our abrupt cut on the injected energies. This way we selected 132 out of the 600 original injections. Fig.6 shows our main results.

From the left and middle panel of Figure 6, we notice that weak(strong) signals are often under(over)-estimated. From the right caption of the same figure we can see that the dispersion of the measurement can be well approximated by a Gaussian. From this Gaussian approximation we can estimate the 90% confidence region of the dispersion histogram. The reason for using a log scale to estimate the confidence region is to avoid negative energy values. Using this method we estimate our energy estimation to be $13_{-7}^{+16}\%$.

D: Co-localization GW151012 and GW151226

During our analysis we were also aware of the results obtained in [29], reporting searches for post-merger signals following GWTC-1 events using the cWB package. Among the analysed events, two of them deserve extra attention: GW151012 and GW151226. According to the authors of [29], these events showed post-merger signals with p-values of $.0037 \pm 0.0014$ and 0.025 ± 0.005 , respectively. However, they concluded that the post-merger signal in GW151012 (despite its low p-value) is unlikely to be originated from the same sky position as the main event. This conclusion was based on the multi-peak structure found for the time-delay distributions of the secondary pulses, but no Bayes factors were calculated to test the co-localization hypothesis. In this section, we address this quantitatively.

We can first reproduce the GW151012 reconstruction performed in [29] (see left panels of Fig.7). We imposed veto to the data (instead of subtraction) in order to exclude the main event, and performed several reconstructions with different search thresholds. The panels in Fig.7 are named according to these thresholds: A-B-C index characterize different search parameter configurations, while the numbers (5 or 3) show the pixel pattern configuration [54] (see [52] for details). The reconstructed waveform shown in the first panel of 7 correspond to the search 5A, with the co-localization analysis in the second panel of the same figure, which can be compared to Figs. 3 and 4 of [29]). Other panels show the maps for different search thresholds. Using Equation (4), we see that all GW151012 searches prefer co-localization of echo and main event, at Bayes factors of 1.6 – 5.4.

E: Bayesian evidence while changing the waveform

To validate that our method has correctly identified echo signals for GW190521, we also test it with a variety of different changes in waveform. As an example, Fig.9 represents posterior plot using the Ringdown waveform (including modes (l,m,n)=(2,2,0), (2,2,1) and (3,3,0)) instead of IMRPhenomXPHM and NRSur7dq4. Table III demonstrates that the Bayesian evidence for stimulated Hawking radiation, is robust to the choice of template. In this table, $\delta_t h_{+/\times}$ implies that we include effect of change in polarisation via change in time delays between the metric polarizations h_+ , h_\times assuming either the strong (beyond GR) gravity regime does [55] change the polarisation of the post-merger signal. Time shift variable in this table accounts for the nonlinear dynamical effects changing the time delay of first echo. The sign variable is \pm in Eq.3.

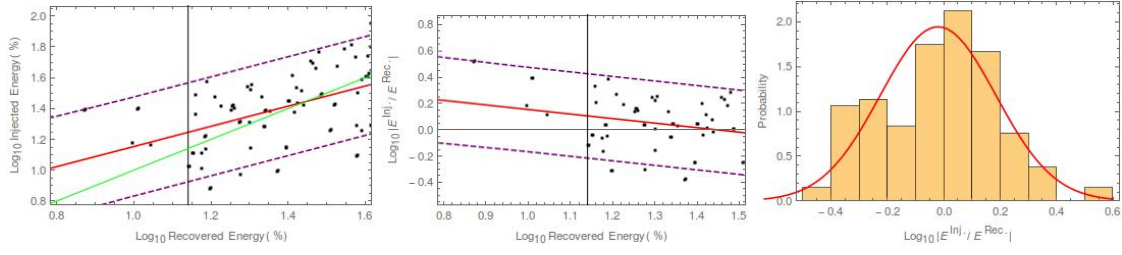


FIG. 6: Left: Energy Plot (log scale). Injected energy as a function of recovered energy for the injection study. The green line is a line of slope 1 for inserted for comparison reasons. Right: Residual Plot (log scale). Difference between recovered and injected energy as a function of recovered energy. Both: Solid red and dashed purple lines represent the best fit of the data to a linear function and its 90% confidence region, respectively. The vertical solid black line marks recovered energy of 13.8%, the value encountered for GW190521. Right: Histogram distribution of the logarithm of the ratio of injected to recovered energy. Our error estimations based on the Gaussian approximation of the histogram lead us to a measurement of $13_{-7}^{+16}\%$ of recovered energy.

$\mathcal{B}^{\text{echoes}}$	7	4	3	5	4	4	4	5	8	8 ± 2	8	6	7 ± 2	6
waveform	IMR	IMR	IMR	R	R	R	IMR	IMR	IMR	R	R	IMR	NR	NR
ϕ	π	$0-2\pi$	$0-2\pi$	$0-2\pi$	$0-2\pi$	$0-2\pi$	$0-2\pi$	$0-2\pi$	π	$0-2\pi$	$0-2\pi$	$0-2\pi$	$0-2\pi$	$0-2\pi$
A	0-1	0-2	0-2	0-2	0-2	0-2	0-1	0-1	0-1	0-2	0-2	0-1	0-2	1
sky location	unif	unif	fixed	unif	fixed	unif	unif	unif	unif	unif	unif	unif	unif	unif
n echoes	3	2	2	2	2	2	3	3	3	2	2	3	2	2
time shift	0	0	0	0	0	± 0.05 sec	0	0	0	0	0	0	0	0
$\delta_t h_{+/\times}$	0	0	0	0	0	0	0	0	0	0	0	$\pm 7\%$	0	0
sign in Eq.(3)	+	+	+	+	+	+	+	-	-	+	-	+	+	+
$\log_{10} \Lambda$	0	0	0	0	0	0	0	0	0	0	0	0	0 ± 13	0 ± 13

TABLE III: Bayes factor for echoes using different GR waveform family and/or echo model. Here IMR stands for IMRPhenomXPHM and R stands for (1,m,n)=(2,2,0), (2,2,1) and (3,3,0) ringdown model [18] and NR stands for NRSur7dq4. The fixed sky location values are chosen for the most likelihood of sky location RA= 3.5 rad (right ascension) and Dec=0.73 rad (declination). “unif” stands for uniform.

F: Cross correlation between detectors

As a complementary test to cWB and PyCBC, we use the method introduced in [28] to correlate the two detectors. Here, instead of Wiener filtering (which is more optimized for signals extended over LIGO bandwidth) we used whitening (dividing data by ASD rather than PSD), and do not add up multiple harmonics. Using the same method introduced in [56] we obtained the amplitude spectral density (ASD). Then we whitened the data by dividing by the ASD.

$$\begin{aligned}
 H(t, f) &= \text{Spectrogram} \left[\text{IFFT} \left(\frac{\text{FFT}(h_H(t-\delta t))}{\text{ASD}_H} \right) \right], \\
 L(t, f) &= \text{Spectrogram} \left[\text{IFFT} \left(\frac{\text{FFT}(h_L(t))}{\text{ASD}_L} \right) \right].
 \end{aligned}
 \tag{15}$$

We implemented the above function based on the same setup as LIGO code [56] to obtain the spectrogram with `mlab.spectrogram()` function in Python with `NFFT=f_s = 16384`, and `mode='complex'`. Similar to [56], the number of points of overlap between blocks is $\text{NOVL} = \text{NFFT} \times$

15/16. Note that with this setup spectrogram uses time ± 0.5 sec in order to Fourier transform around each time.

The resulting spectrogram is cross-correlation of two detectors H1 and L1,

$$X(t, f) = \Re [H(t, f) \times L^*(t, f)], \tag{16}$$

which is the whitened cross-power spectrum of the two detectors. Taking into account the opposite phase of GW polarization for Hanford and Livingston, the real signals show up as peaks in $X(t, f)$.

G: Effective time delay between Hanford and Livingston

We find the time delay δt between the two detectors via a naive estimation, explained in the following:

1. One of the whitened strain series is shifted within (-10 msec, 10 msec).
2. A complex spectrogram for both Hanford and Livingston detectors, $H(t, f)$ and $L(t, f)$ with 16k Hz data is obtained.

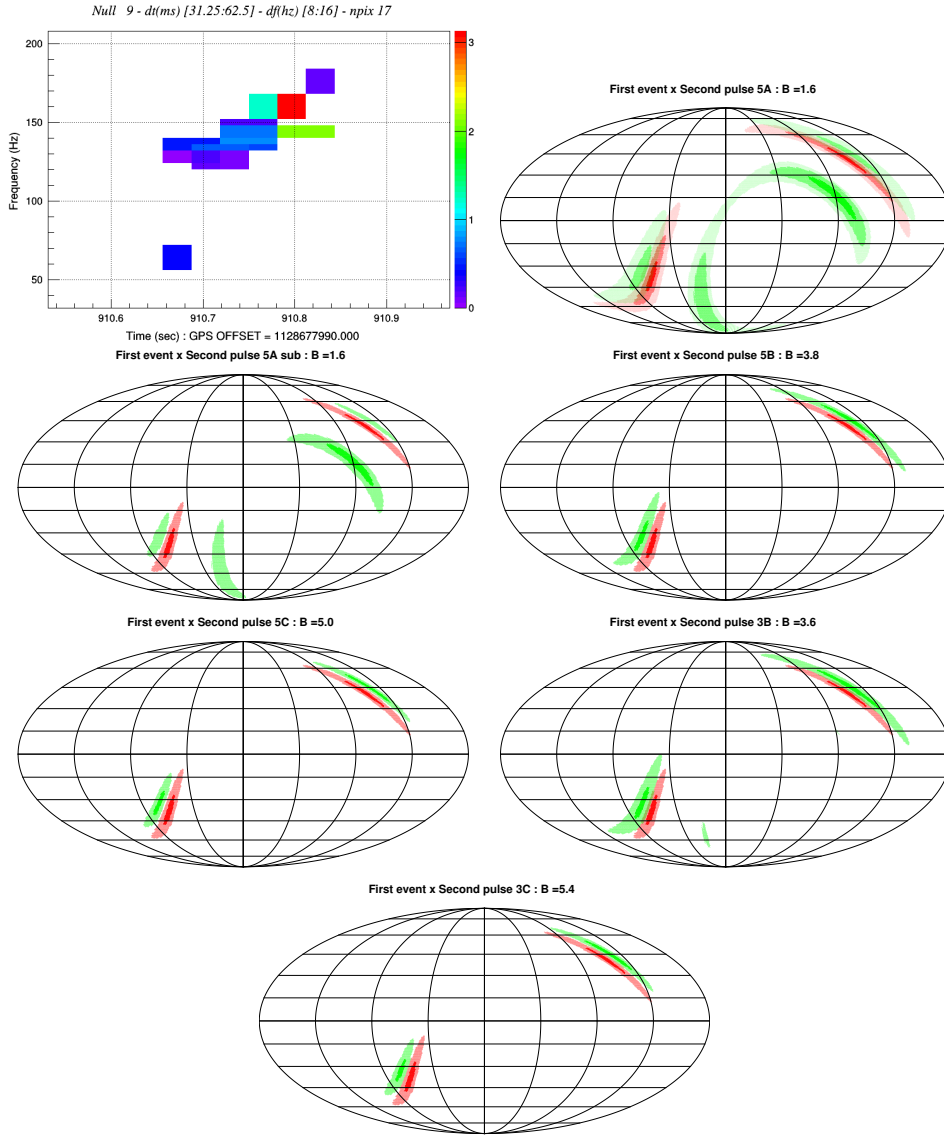


FIG. 7: Co-localization analysis for GW151012. We performed several reconstructions with different search thresholds. The panels are named according to their thresholds: A-B-C index relates with different search parameters configurations and the numbers (5 or 3) relates pixel pattern configuration [54]. All searches prefer the hypothesis of sky co-localization of echoes and main event, at Bayes factors of 1.6-5.4.

3. Since the two detectors H1 and L1 have nearly 180 degrees phase difference, we maximized $|H(t - \delta t, f) - L(t, f)|$ for constant f within the range $t - t_{\text{merger}} = (-2 \text{ s}, +0.6 \text{ s})$ and $f = (35 \text{ Hz}, 100 \text{ Hz})$.
4. We only kept the 10 highest values of $|H(t - \delta t, f) - L(t, f)|_{f=f_{\text{max}}(t)}$ and sum over them (we expect smaller values to be affected by noise).
5. Finally, δt is found having the maximized value of

this sum, which happens at the value of 1.71 ms.

Note that, the time delay $\delta t = 1.71 \text{ ms}$ is not a precise geometric time delay and is affected by small phase differences away from 180 degrees between the two detectors as well. Interestingly, precise calculation with fix maximum likelihood sky location values of $\text{ra}=3.5 \text{ rad}$ and $\text{dec}=0.73 \text{ rad}$ corresponds to the detector time difference of 1.62 ms consistent with what has been obtained in this section.

Here Fig.10 represents result of this method in wider range in comparison to Fig.1.

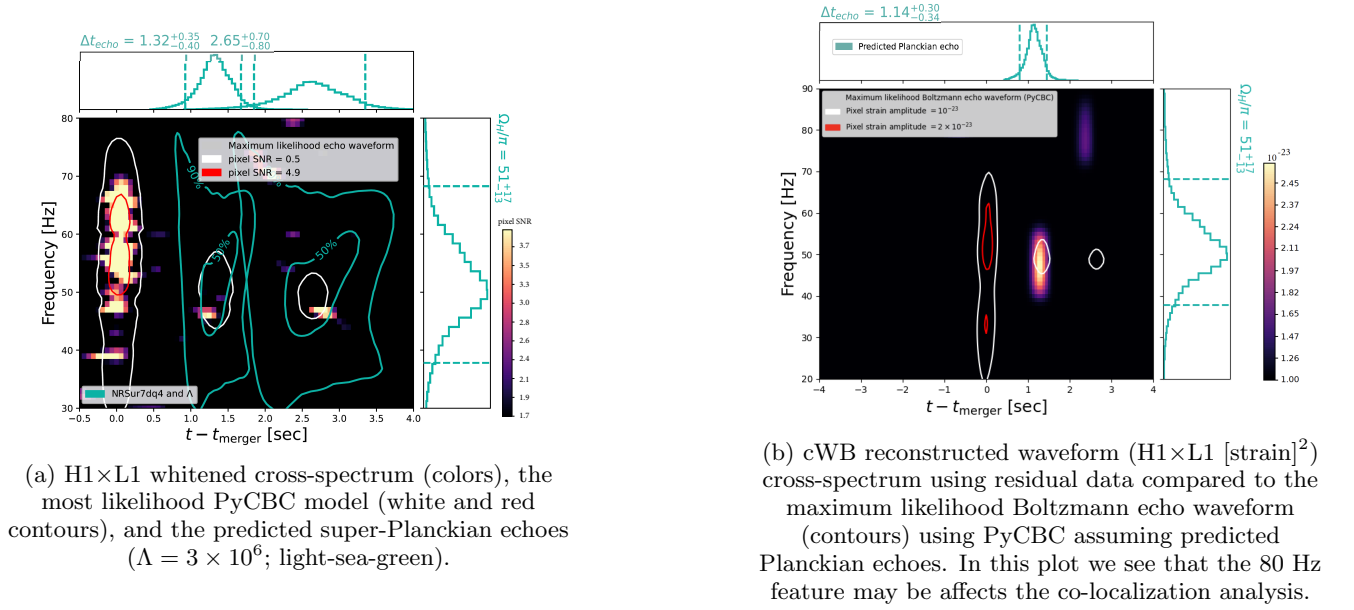


FIG. 8: Comparison of three search methods: PyCBC, Cross-correlation, and cWB. White and red contours represent maximum likelihood Boltzmann echoes based on NRSur7dq4 general relativistic surrogate model. Contours with light-sea-green color represent 50% and 90% expected regions along with their 1D distributions, for both 1st and 2nd echoes.

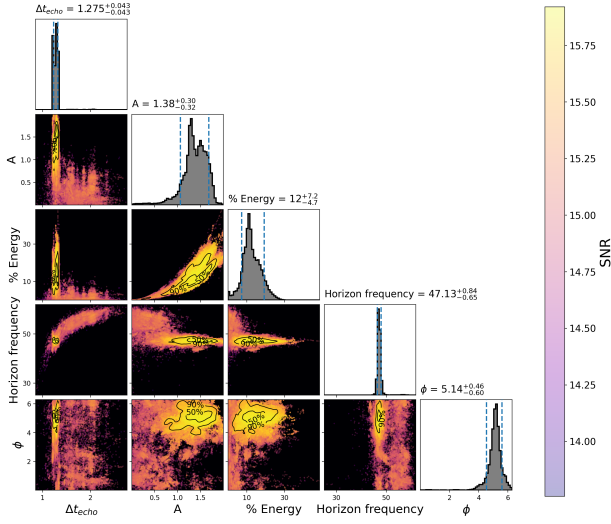


FIG. 9: Parameter estimation of Ringdown+(Boltzmann) Echoes waveform for GW190521. This plot has shown $\mathcal{B}^{\text{Echoes}} = 8 \pm 2$ in preference for Boltzmann echoes waveform. Contours in Off-diagonal plots indicate the 50% and 90% credible regions of 2D marginal posteriors. The diagonal plots show the 1D marginal posteriors, with the median and 90% credible intervals where the recovered values are indicated at top of the plots.

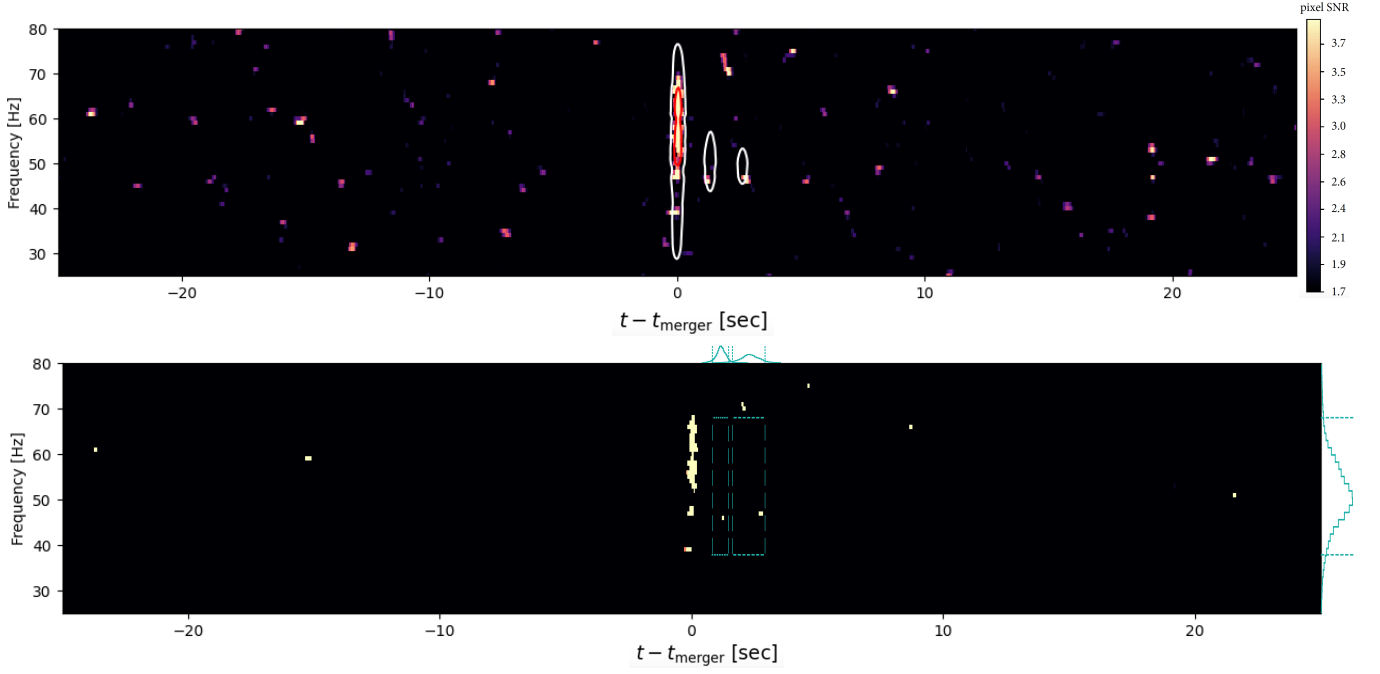


FIG. 10: Look-elsewhere plot demonstrating that the echo signals found within Planckian 1st and 2nd echo contours are scarce in random noise. a) Same cross-correlation of H1 and L1 as Fig.1 with extended time of $-25 \text{ sec} \leq t - t_{\text{merger}} \leq +25 \text{ sec}$ for GW190521 based on Eq.16. b) Cross-correlation of H1 and L1 except for fixed pixel power corresponding the first echo pixel and 1D distributions show predicted 1st and 2nd Planckian echoes and horizon frequency.